Journal of Molecular Structure 1270 (2022) 133949

Contents lists available at ScienceDirect

Journal of Molecular Structure

journal homepage: www.elsevier.com/locate/molstr

Synthesis, X-ray crystal structure of Cu(II) 1D coordination Polymer: In View of Hirshfeld surface, FMO, Molecular electrostatic potential (MEP) and Natural Bond orbital (NBO) analyses

Mridula Guin[a], Shibashis Halder[b], Sudipta Chatterjee[c], Saugata Konar[d,*]

[a] Department of Chemistry and Biochemistry, Sharda University, Greater Noida, Uttar Pradesh 201310, India
[b] Department of Chemistry, Tej Narayan Banaili College, Bhagalpur, Bihar 812007, India
[c] Department of Chemistry, Serampore College, Serampore, Hooghly, 712201, India
[d] Department of Chemistry, The Bhawanipur Education Society College, Kolkata 700020, India

ARTICLE INFO

Article history:
Received 9 February 2022
Revised 4 August 2022
Accepted 13 August 2022
Available online 14 August 2022

Keywords:
1D Cu(II) complex
X-ray crystal structure
DFT
Hirshfeld surface analysis
NBO, MEP

ABSTRACT

A dynamic area in the realm of contemporary scientific research is the synthesis of molecular systems that exhibit binding abilities for the creation of effective coordination polymeric structures. In addition to the varied network architecture, the rational design and synthesis of metal-organic coordination polymers is currently of great interest because these extended polymeric systems are vital to numerous fields of modern research. In this present research, a new 1D coordination polymer of Cu(II) complex $[Cu_2(mPzA)_2(Bz)]_n$ (**1**) has been synthesized using two different ligands i.e. 5-methyl-pyrazole-3-carboxylic acid (mPzA) and benzoic acid (Bz). X-ray crystallography study reveals that in the solid-state structure of the title complex, Cu(II) exhibits distorted trigonal bipyramidal geometry. Quantum chemical calculations using density functional theory (DFT) method have been carried out for the complex **1**. The computed results further support the experimental findings of the complex adopting a square pyramidal geometry. In the basal plane, the copper atom is bonded through two nitrogen atoms and two oxygen atoms which are bridged between two copper atoms. The axial position is occupied by the oxygen atom of a carboxyl group. Frontier molecular orbital analysis using the global reactivity parameters demonstrates the compound to be stable and less reactive. Moreover, molecular electrostatic potential (MEP) is evaluated using the electron density of the compound to predict the reactive sites. The MEP map clearly indicates strong electrophonic reaction potential of this complex. Natural bond orbital (NBO) analysis has been performed to check the hyperconjugation and thereby stability of the complex **1**. NBO analysis revealed the charge delocalization from the bridging oxygen atoms towards copper atoms. The Hirshfeld surface analysis demonstrates absence of $\pi\cdots\pi$ stacking interaction and significant contribution of H···H (39.7%) and O···H (24.1%) interactions in building the supramolecular crystal packing.

1. Introduction

The development of molecular systems that exhibits binding abilities for the construction of efficient coordination polymeric frameworks continues to be an active area in the field of scientific research. Not only because of the varied network topology, but also because these extended polymeric systems are essential for catalysis [1,2], luminescence [3,4], magnetism [5,6], nonlinear optics [7,8], adsorption, and separation [9,10], rational design and synthesis of metal-organic coordination polymers is currently of great interest. A variety of elements play a significant role in this situation, including the core metal ions [11], organic ligands [12], metal-ligand ratio [13], solvents [14], temperature [15], pH value [16], counter ions [17], and templates [18]. The sensible selection of an organic building block and metal centre is amongst them, and it is one of the most important aspects in the synthesis of coordination polymers. In our approach, coordination polymers have been built using O- or N-donor ligands. In this sense, the flexible ligand 5-methyl-pyrazole-3-carboxylic acid (mPzA) is a class exemplar. The addition of well-designed auxiliary ligands has accelerated the structural evolution that has produced complexes with a range of nuclearities. As the coordination properties of metals vary depending on the circumstances, it is frequently challenging to tune the products produced in a multi-ligand reaction. Thus,

* Corresponding author.

https://doi.org/10.1016/j.molstruc.2022.133949
0022-2860/

adding or changing functionalities to the carboxylate ligand can change the final products' ability to aggregate. Because of their adaptable coordination capabilities, pyrazole-based ligand planning and application have been prioritised. Because it may adopt a variety of coordination modes in conjunction with O- or N-donor ligands, Cu(II) is a well-known candidate for the development of metal-organic materials [19,20].

Moreover, prediction of the electronic structures of transition metal complexes using density functional theory (DFT) method is an admired method utilized by the global scientific community. It assists in interpreting and elucidating molecular structure and properties in a supportive way. Various properties computed from the energy gap between HOMO and LUMO, play pivotal role in understanding the potential of any compound for its application in biomedical field and several other applications. In addition to that molecular electrostatic potential is an important descriptor in recognizing the polarity and reactivity of a compound. MEP can precisely determine numerous types of molecular interaction in terms of hydrogen bonding, enzyme-substrate or drug-receptor interactions. The donor acceptor interactions and charge delocalization of the complex is explored using NBO analysis. Molecular Hirshfeld surface analysis [21] assists in visualizing intermolecular interactions and packing modes of a crystal by surface contours in terms of d_{norm}, shape index and curvature. Two dimensional finger print plots are used to evaluate the contributions of various close contacts in crystal packing.

Taking advantage of this understanding, herein, we report the synthesis and X-ray characterization of new 1D coordination polymer of Cu(II) complex (**1**) with two different ligands i.e. 5-methyl-pyrazole-3-carboxylic acid (mPzA) and benzoic acid (Bz). In this work, we have utilized 5-methyl-pyrazole-3-carboxylic acid (mPzA) bearing a flat pyrazole ring with two nitrogen and carboxylate oxygen donor atoms, encouraged by the coordinative versatility offered by the use of benzoic acid (Bz) as an ancillary ligand as carboxylate connector. So, herein we present one new CP (Coordination polymer) namely $[Cu_2(mPzA)_2(Bz)]_n$ characterized using X-ray crystalography and DFT method. Moreover, Hirshfeld surface analysis is performed to understand crystal packing and types of intermolecular interactions involved in stabilizing the molecular crystal.

2. Experimental methods

2.1. General methods and materials

All reagents and chemicals were of AR grade and obtained from commercial sources (SD Fine Chemicals, India; and Aldrich) and used without further purification.

2.2. Physical measurements

IR spectra were recorded in the region 400–4000 cm^{-1} using a Perkin–Elmer model 883 infrared spectrophotometer. Elemental analyses (C, H and N contents) were carried out by a Perkin–Elmer CHN analyser 2400 at the Indian Association for the Cultivation of Science, Kolkata. The electronic spectra of the complexes in methanol solution were recorded on a Hitachi model U-3501 spectrophotometer.

2.3. Synthesis

2.3.1. Synthesis of 5-Methyl pyrazole 3-Carboxylic acid (mPzA)

The ligand **'mPzA'** was synthesized by reported method [22].

2.3.2. Synthesis of $[Cu_2(mPzA)_2(Bz)]_n$ (1)

A methanolic solution (10 cm^3) of $Cu(ClO_4)_2{\cdot}6H_2O$ (1 mmol, 0.370 g) was added dropwise to a solution of mPzA (1 mmol, 0.126 g) in the same solvent (20 cm^3) taken in a 1:1 M ratio with constant stirring, and after 30 mints. 5 cm^3 aqueous solution of benzoic acid (1 mmol, 0.122 g) was added dropwise continued for two additional hours. The solution turned deep blue. After stirring, it was left for slow evaporation at room temperature. After 2 weeks X-ray quality crystals of **1** separated out and they were collected by the usual technique. (Yield: 71%). Elemental analysis: anal. calc. for $C_{17}H_{13}Cu_2N_4O_6$: C, 41.00; H, 2.61; N, 11.28. Found: C, 40.57; H, 2.58; N, 11.29%. IR bands (KBr pellet, cm^{-1}): 2086 (s), 1591 (m), 1629 (s), 747 (m).

Table 1
Crystal data for **1**.

Formula	$C_{17}H_{13}N_4O_6Cu_2$
Formula weight	496.41
Crystal system	Monoclinic
Space group	C 2/c
a/Å	19.2686(16)
b/Å	10.7492(7)
c/Å	13.2592(8)
α/°	90.00
β/°	101.920(4)
γ/°	90.00
V/Å^3	2687.1(3)
Z	4
D_c/g cm^{-3}	1.227
μ/mm^{-1}	1.613
$F(000)$	996
θ range/°	2.16–24.92
Reflections collected	13,243
Unique reflections	2339
Reflections $I > 2\sigma(I)$	1977
R_{int}	0.0259
Goodness-of-fit (F^2)	1.057
R_1 ($I > 2\sigma(I)$)[a]	0.0319
wR_2[b]	0.0642
$\Delta\rho$max/min/e Å^3	−0.21, 0.29

[a] $R_1 = \Sigma||F_o| - |F_c||/\Sigma|F_o|$.
[b] $wR_2 = [\Sigma(w(F_o^2 - F_c^2)^2)/\Sigma w(F_o^2)^2]^{1/2}$.

2.4. X-ray crystallography study

A suitable single crystal of **1** was mounted on the tip of a glass fibre coated with commercially available super glue. X-ray single crystal data were collected at room temperature using a Bruker APEX II diffractometer, equipped with a fine-focus, sealed tube X-ray source with graphite monochromated Mo-Kα radiation (λ = 0.71073 Å). The data were integrated using a SAINT program [23] and absorption correction was made with SADABS. The structure was solved with the help of SHELXT [24] following direct methods and refined by full matrix least-squares on F2 using SHELXL-2014/7 [25] with anisotropic displacement parameters for all non-hydrogen atoms. All the hydrogen atoms were fixed geometrically and placed in ideal positions. Data collection and structure refinement parameters are given in Table 1.

2.5. Density functional theory (DFT) study

Elucidation of the electronic structure of the complex is performed through Density Function Theory (DFT) calculations using Gaussian 16 program package [26]. DFT calculations using hybrid functional deliver excellent computational accuracy with limited computational cost. The geometry optimization was carried out by B3LYP functional with 6–31 G + LANL2DZ (Los Alamos National Laboratory 2 Double-Zeta), mixed basis set that utilizes Los Alamos Effective core potential on the transition metal Cu while a Pople basis set has been used for all other atoms. The convergence criteria were maintained at default level without any constraint on

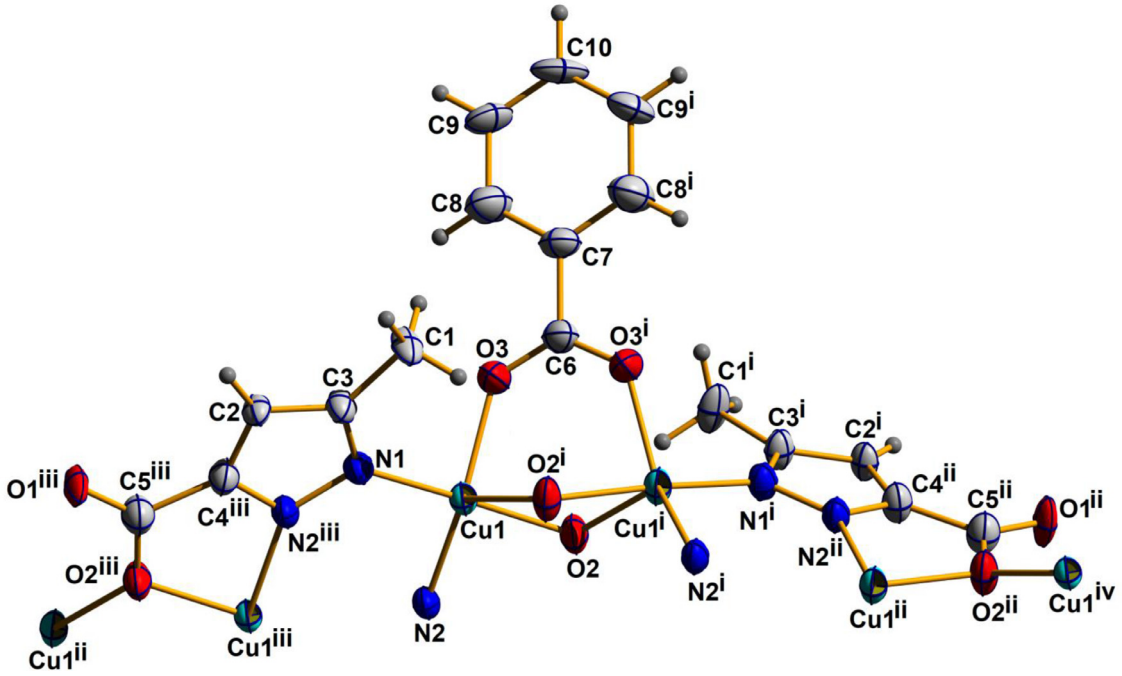

Fig. 1. ORTEP diagram of complex **1** drawn with 50% ellipsoidal probability. Symmetry codes: (i) - x, y, 5-z; (ii) x, -y, 0.5 + *z*; (iii) - x, -y, 1 - z; (iv) - x, -y, 2-z.

the geometry. Absence of negative frequency suggests the molecule to be a true minimum on the potential energy surface. Energy of HOMO and LUMO is determined to understand the chemical reactivity of the compound. Moreover molecular electrostatic potential of the compound is calculated from the electron density to predict its reactive sites. Natural bond orbital (NBO) analysis have been performed using NBO program [27] as implemented in Gaussian 16 program package to investigate the direction and magnitude of the donor-acceptor interactions in the complex. The interaction strength between filled orbital of the donor (ϕ_i) and the empty orbital of the acceptor (ϕ_j) has been determined by second order perturbation energy.

2.6. Hirshfeld surface analysis

Crystal Explorer 17.5 program [28] was used to analyse Hirshfeld surface (HS) of the compound in order to find out various intermolecular interactions in the crystal. The Hirshfeld surface mapped over d_{norm} in the range of −1.1647 to 3.1637 a.u. highlighting the close contacts using a red-blue-white colour coded scheme. A high surface resolution was adopted in calculating the HS. Moreover, Hirshfeld surface mapping of shape index to determine the presence of π-π stacking interaction and curvedness to find the coordination of individual atoms in the crystal was also performed. The calculated surfaces are presented with surface transparency to enable clear visualization. Further 2D fingerprint (FP) plots were calculated to summarize the nature and type of intermolecular contacts and the contribution of different intermolecular contacts towards crystal packing.

3. Results and discussion

3.1. Crystal structure descriptions of complex 1

Compound **1** is crystallized in the C 2/c space group. A perspective view of complex **1** is shown in Fig. 1. Table 2 contains the selected bond lengths and bond angles of complex **1**. The asymmetric unit contains a penta-coordinated copper centre exhibiting geometry very close to highly distorted trigonal bipyramidal characterized by addition parameter, τ = 0.58 of Cu1 (where τ = 0 and 1 for perfect square pyramidal and trigonal bipyramidal geometries, respectively) [29]. The five co-ordinations of copper are fulfilled by O3 of the carboxyl group attached to benzene ring, two oxygen atoms (O2) of carboxyl group attached to pyrazole ring and, N1 and N2 from pyrazole moiety. The O2 oxygen is functioning as a bridge between two adjacent copper centers and that oxygen atom helps for growing up the 1D coordination polymer. The Cu1–N1, Cu1–N2, Cu1–O2 and Cu1–O3 bonds lengths are 1.9434 Å, 1.9717 Å, 1.985 Å and 2.0054 Å respectively. N1–Cu1–N2, N1–Cu1–O2, N2–Cu1–O2, N1–Cu1–O3, N2–Cu1–O3 and O2–Cu1–O3 angles are 100.03°, 174.92°, 81.05°, 93.62°, 139.97° and 88.62° respectively. These asymmetric units are connected to each other to generate one dimensional chain. The dihedral angle (on the basis of copper-pyrazole moiety and copper-benzoic acid moiety) with respect to one copper atom is 57.47° Two adjacent one dimensional chains are interconnected with weak Vander-Waals interactions.

3.2. Geometry optimization and electronic structure

The optimized geometry of the complex with atomic label is shown in Fig 2. The geometrical parameters of the complex along with the crystallographic data are listed in Table 2. The computed geometrical parameters are found to be in well accordance with the experimental data. Slight mismatch in few cases might be due to the phase difference in experiment and computation.

3.3. Frontier molecular orbital (FMO) analysis

In addition, various electronic properties for example energy of highest occupied molecular orbital (E_{HOMO}) and lowest unoccupied molecular orbital (E_{LUMO}), Energy difference (E_{gap}) between HOMO and LUMO orbitals were also computed. In accordance with Koopman's theorem [30], ionization potential (I) and electron affinity

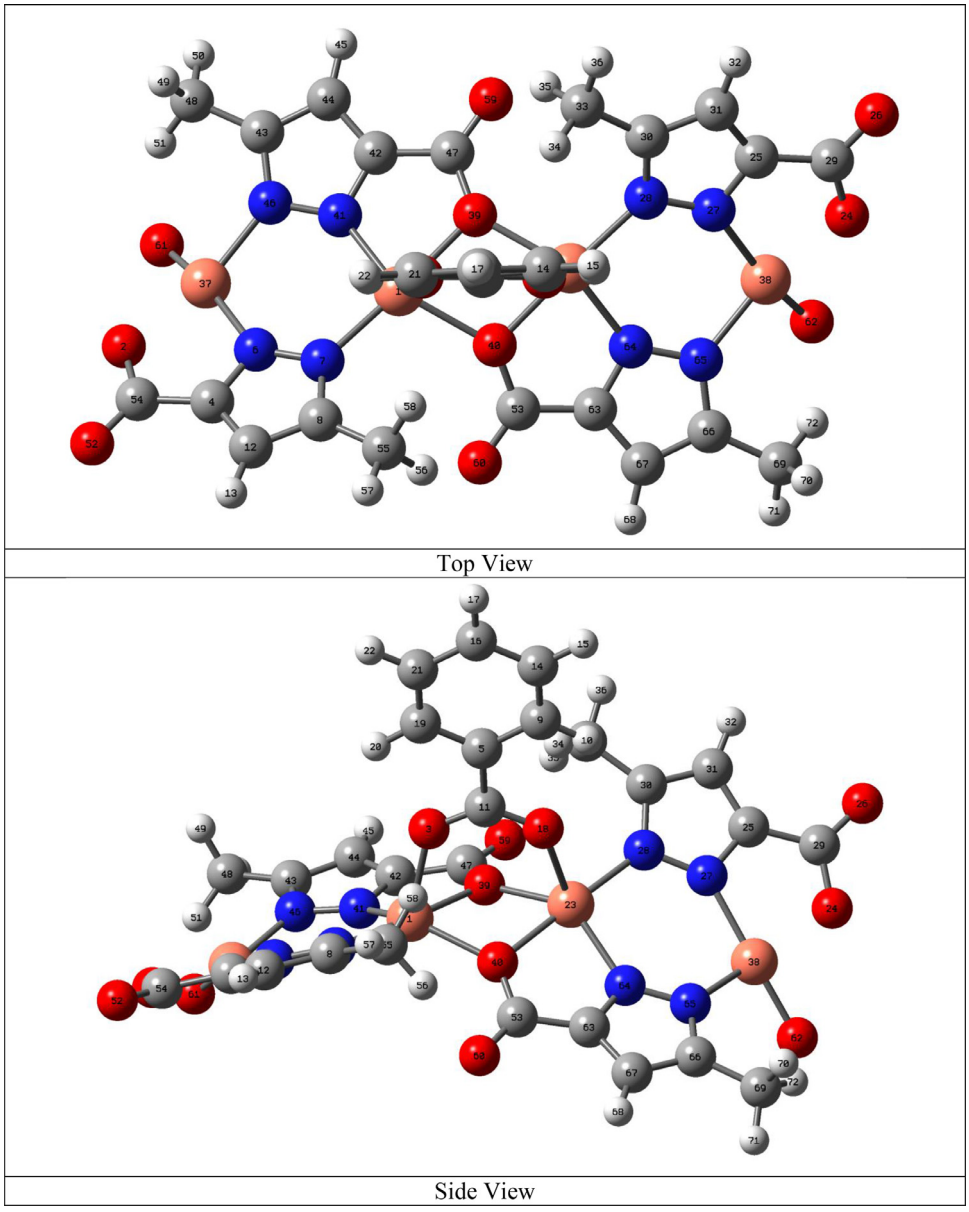

Fig. 2. Optimized geometry of the complex **1**.

(A) of a molecule is related to E_{HOMO} and E_{LUMO}. Various other reactivity parameters such as global hardness (η), softness (S), electronegativity (χ), Chemical potential (μ) and electrophilicity index (ω) of the compound are calculated and the corresponding values are listed in Table 3.

The calculated 3D plots of frontier orbitals HOMO and LUMO with the energy gap is shown in Fig. 3. The computed energy gap 0.718 eV suggests the compound to be less polarized and stable entity. A stronger interaction is facilitated when target molecule with high HOMO energy acts as electron donor with interacting molecule as acceptor with lower LUMO energy. The global reactivity descriptors explain the chemical reactivity and kinetic stability of the compound. Higher the value of the global hardness, lower is the reactivity while higher value of global softness indicates higher reactivity. The observed value of η and S indicates the compound to be chemically less reactive.

3.4. Molecular electrostatic potential (MEP)

The molecular electrostatic potential (MEP) of the complex is computed using the electron density of the molecule and displayed in Fig. 4. The MEP diagram indicates the electrophilic and nucleophilic active sites of the complex on the basis of electron density. The increasing order of electrostatic potential is indicated in the colour scale from red to blue. The green colour is associated with region where potential is zero. It can be seen from the MEP map, the region with oxygen atom of the carboxyl group is observed as orange to yellow shed. These are the sites of strong electrophilic reactivity of the compound **1**. While the regions with blue colour associated with positive electron density for nucleophilic reactivity are almost nil in this complex. The result of MEP map clearly indicates electrophonic reaction potential of this complex through the carboxyl group linked to the pyrazole ring.

Table 2
Selected bond lengths and bond angles.

Selected bonds	Bond lengths (Å)	
	XRD	DFT
Cu1–N1	1.9434(16)	1.9761
Cu1–N2	1.9717(16)	2.0557
Cu1–O2 (non-bridged)	1.9850(13)	1.9877
Cu1–O2 (bridged)	2.2274 (14)	2.0881
Cu1–O3	2.0054(15)	2.2217
O2–C5	1.287(3)	1.3311
O3–C6	1.2586(19)	1.2857
C4–N2	1.336(2)	1.3591
C4–C2	1.382(3)	1.3999
C4–C5	1.486(3)	1.4802
O1–C5	1.219(3)	1.2601
C7–C8	1.384(3)	1.4037
C7–C6	1.503(4)	1.5196
N2–N1	1.363(2)	1.3695
N1–C3	1.350(3)	1.3727
C3–C2	1.381(3)	1.4046
C3–C1	1.497(3)	1.4940
C8–C9	1.380(4)	1.3989
C6–O3	1.2586(19)	1.2857
C9–C10	1.367(4)	1.4016
Selected bond angles	**Bond angles (°)**	
	XRD	DFT
N1–Cu1–N2	100.03(7)	98.60
N1–Cu1–O2	174.92(7)	177.30
N1–Cu1–O2	97.32 (6)	109.43
N2–Cu1–O2	81.05(6)	82.27
N2–Cu1–O2	123.69(6)	138.21
O2–Cu1–O2	78.05(6)	73.51
N1–Cu1–O3	93.62(7)	93.04
N2–Cu1–O3	139.97(6)	118.86
O2–Cu1–O3	88.62(6)	86.35
O2–Cu1–O3	91.10(6)	90.78
C5–O2–Cu1	116.70(13)	115.35
C5–O2–Cu1	135.49(14)	115.34
Cu1–O2–Cu1	98.03(6)	103.76
C6–O3–Cu1	129.69(16)	128.10
C4–N2–Cu1	113.00(13)	112.07
C3–N1–Cu1	131.18(14)	131.33
N2–C4–C5	116.07(18)	116.69
C4–N2–N1	107.75(15)	108.44
N1–N2–Cu1	138.76(12)	139.45
C3–N1–N2	108.03(16)	108.30
N2–N1–Cu1	120.79(12)	120.09

Table 3
FMO energy parameters and global reactivity descriptors of the compound **1**.

Parameters	Values
HOMO (eV)	1.569
LUMO (eV)	2.287
ΔE = (LUMO–HOMO) (eV)	0.718
I = -E(HOMO)(eV)	−1.569
A = -E(LUMO) (eV)	−2.287
$\chi = (I + A)/2$ (eV)	−1.928
μ = - χ (eV)	1.928
χ = (I - A)/2 (eV)	0.359
$S = 1/\chi$ (eV)	2.785
$\omega = \mu^2/2\ \chi$ (eV)	5.177

3.5. Natural bond orbital (NBO) analysis

Natural Bond orbital (NBO) analysis has been performed on the optimized geometry of the complex using NBO program. Natural atomic charges, total natural populations, natural electronic configurations and Wiberg bond indices of the complex is determined and reported in Table 4. The data in Table 4 indicates that the valence orbital of both copper atoms is characterized by 5p. The atomic charges for the atoms that are involved in metal-ligand bonds are listed in the same table. The oxygen atoms linking the two copper atoms have the lowest atomic charge suggesting charge delocalization mostly happens from these atoms towards the Cu metal. Wiberg bond indices (WBI) of selected atoms are calculated to determine the nature of various bonds involving with the coordination with copper atom. The values of WBI are similar for Cu-N bonds that are positioned trans to each other. For example Cu1-N7 and Cu23-N28 have similar WBI and in the same way, Cu1-N41 and Cu23-N64 have similar WBI value. However WBI of Cu1-N7 and Cu23-N28 are higher than Cu1-N41 and Cu23-N64. This implies that Cu1-N7 and Cu23-N28 are weakly covalent and are shorter than the Cu1-N41 and Cu23-N64 bond. The axially positioned Cu-O bonds e.g. Cu1-O3 and Cu23-O18 have WBI of 0.0854 indicating a very long and weak bond. The electronic charge transfer from the filled orbitals to the vacant orbital indicates intramolecular delocalization. The strength of these hyperconjugative interactions are calculated using second order perturbative analysis of the Fock matrix. NBO analysis data is presented in Table S1. The stabilization of the complex is arising due to the hyperconjugative interactions between the orbitals of LP(1) C8→π^* N6-N7, LP(1) C30→π^* N27-N28, LP(1) C43→π^* N41-N46 and LP(1) C66→π^* N64-N65 with large E^2 values ranging from 750 to 973 kcal/mol. These intense charge transfer interactions primarily contribute towards the stabilization of the molecular complex.

3.6. Hirshfeld surface analysis

Numerous researches are reported on understanding metal-ligand interaction using Hirshfeld surface analysis [31–35]. The role of Hirshfeld surface analysis for 1D polymer complex based on Cu(II) ion [31,32], Cd(II), Ba(II), Co(II) [33] and many other metal ions clearly establish its potential to understand structure-property relationships in crystalline material.

The Hirshfeld surfaces of the polymeric compound consisting of three molecules were mapped in terms of d_{norm}, curvedness and shape index and are shown in Fig. 5. Three molecules are chosen for the calculation to reduce the computational cost. We have further performed calculation with five molecules to understand the if it affects Hirshfeld surface analysis results. The d_{norm} surfaces are splitted into regions with different colour codes. The region with red colour represents a negative electrostatic potential surface whereas the region with blue colour indicates a positive electrostatic potential surface. d_{norm} is defined as the ratio of normalized contact of any point in the surface to the nearest interior (di) and exterior (de) atom and the VDW radii of the atom. The slightest modification in the surface shape will be highlighted by the shape index. The curvedness denotes the curvature of the molecule to understand planar packing modes in the crystal. 2D fingerprint (FP) plots delineated into various individual intermolecular contacts have been determined. The quantitative description of specific atom—atom contacts in a crystal is clearly shown in the fingerprint plots.

The d_{norm} mapping of the complex is shown in Fig. 5(a). The big red spots in the d_{norm} mapping are due to the formation of close contact through N···N intermolecular interactions. The shape index [Fig. 5(b)] exhibit few red triangles in the concave regions that signify the atoms that stacked above the plane of surface and blue triangles in the concave regions indicate atoms inside the surface. Absence of adjacent red and blue triangles suggests that crystal is not packed with π-π stacking interactions. The curvedness mapping [Fig. 5(c)] also indicates the packing modes of the crystal. Similar to shape index mapping, the signature of curvedness

Table 4
Natural atomic charges, total natural populations, natural electronic configurations and Wiberg bond indices of selected atoms in the compound **1**.

Atom	Charge	TNP	Natural electronic configuration	Bond	WBI
Cu1	1.25276	27.74724	Cu1[*core*]$4s^{0.28}$ $3d^{9.45}$ $4p^{0.01}$ $5p^{0.01}$	Cu1-O39	0.1837
O39	−0.77485	8.77485	O39[*core*]$2s^{1.75}$ $2p^{5.01}$ $3p^{0.01}$	Cu1-O40	0.1862
O40	−0.77204	8.77204	O40[*core*]$2s^{1.75}$ $2p^{5.01}$ $3p^{0.01}$	Cu1-O3	0.0854
O3	−0.74381	8.74732	O3[*core*]$2s^{1.73}$ $2p^{5.01}$	Cu1-N7	0.2043
N7	−0.40306	7.40306	N7[*core*]$2s^{1.37}$ $2p^{4.01}$ $3p^{0.02}$	Cu1-N41	0.1557
N41	−0.40519	7.40519	N41[*core*]$2s^{1.38}$ $2p^{4.00}$ $3p^{0.02}$	Cu23-O39	0.1841
Cu23	1.24365	27.75635	Cu1[*core*]$4s^{0.28}$ $3d^{9.46}$ $4p^{0.01}$ $5p^{0.01}$	Cu23-O40	0.1816
O18	−0.74361	8.74361	O18[*core*]$2s^{1.73}$ $2p^{5.01}$	Cu23-O18	0.0854
N28	−0.40106	7.40106	N28[*core*]$2s^{1.37}$ $2p^{4.01}$ $3p^{0.02}$	Cu23-N28	0.2013
N64	−0.39938	7.39938	N64 [core]$2s^{1.38}$ $2p^{3.99}$ $3p^{0.02}$	Cu23-N64	0.1538
C47	0.75248	5.24752	C47[*core*]$2s^{0.76}$ $2p^{2.45}$ $3p^{0.04}$	O39-C47	1.1332
C53	0.75123	5.24877	C53[*core*]$2s^{0.76}$ $2p^{2.45}$ $3p^{0.04}$	O40-C53	1.1359

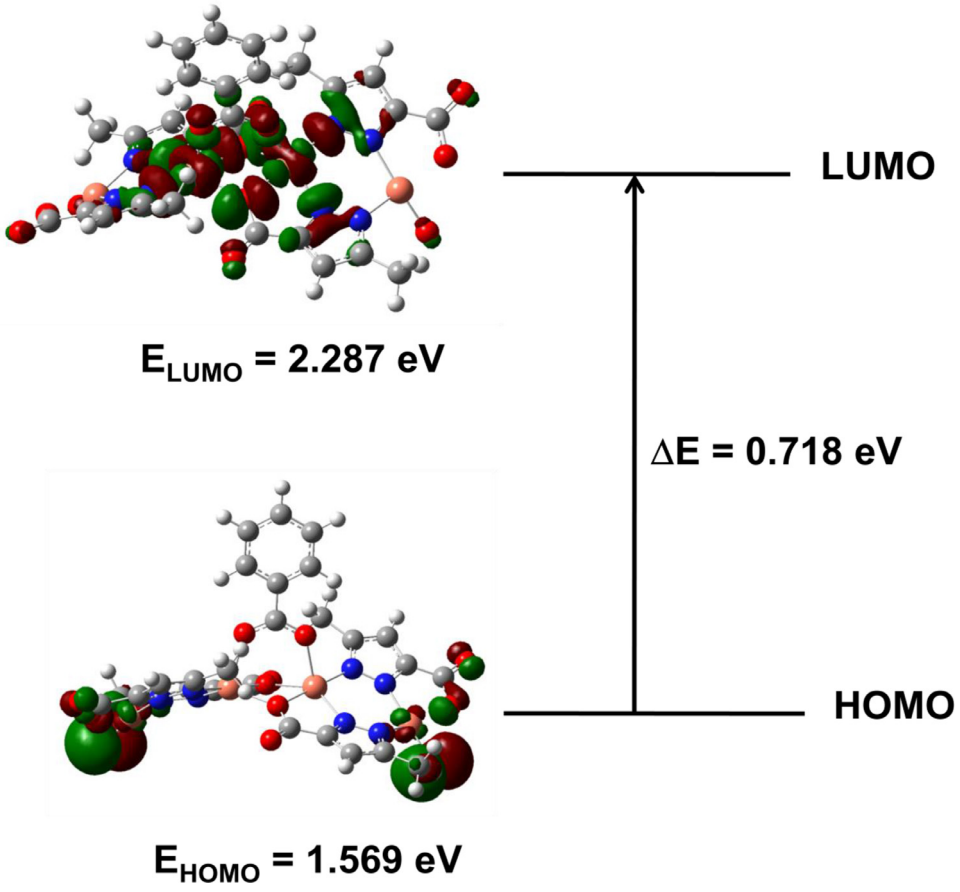

Fig. 3. 3D plots of HOMO and LUMO and energy gap of the compound.

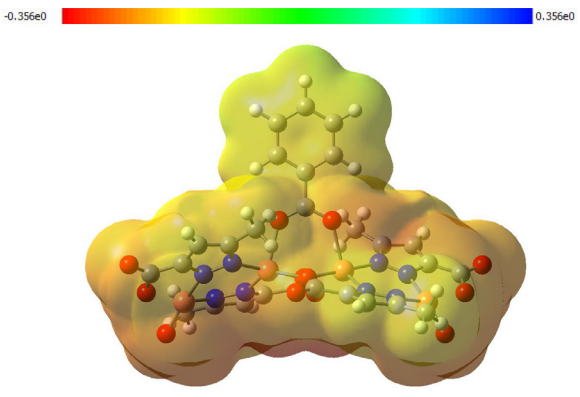

Fig. 4. Molecular electrostatic potential surface of the complex **1**.

also reveal that π-π stacking interactions are weak in this crystal packing [36]. The intermolecular interaction of N···N contacts on the Hirshfeld surface is shown in Fig. 5(d).

The two dimensional fingerprint plots of the major intermolecular contacts the title compound is shown in Fig. 6. The two most significant contacts stabilizing the molecular crystal are H···H and O···H interactions with percentage contribution of 39.7% and 24.1% respectively to the overall crystal packing. The other significant interactions are C···H with 15.8%, N···H with 7.0% and C···O with 4.4% contribution. Further, C···C, C···N and N···N interactions have minor contribution towards the crystal packing. The absence of characteristic bow-tie patterns in the FP plot of C···H contacts indicates absence of $\pi-\pi$ stacking interaction [37,38]. Further, very less percentage contribution of C···C contacts (1.3%) which is primarily involved in $\pi\cdots\pi$ stacking, proves

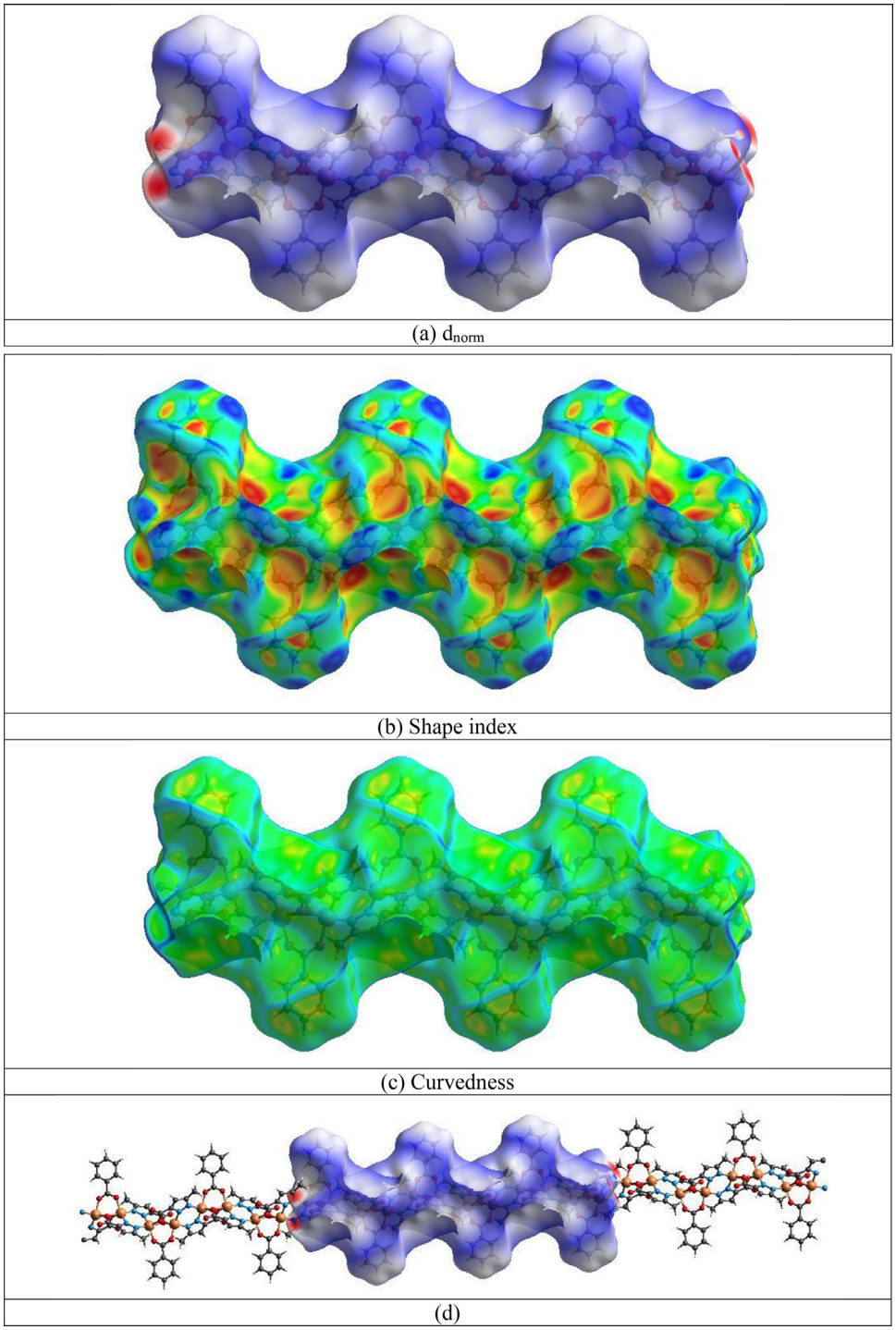

Fig. 5. Hirshfeld surfaces mapped over (a) d_{norm}, (b) shape index and (c) curvedness (d) intermolecular interaction through N···N contacts on the Hirshfeld surface.

the absence of such $\pi-\pi$ stacking interaction in packing of the crystal. The Hirshfeld surface analysis reveals H···H and O···H interaction as the primary structural features in constructing the supramolecular arrangement of the crystal. In addition to that N···N contacts control the solid state packing of the molecular crystal along X-axis. To understand whether the number of monomer units present in the compound affect the Hirsfeld surface analysis results, we have also performed the calculation using five molecules in the polymeric compound. The mapped surfaces are shown in Fig.S1 and the FP plots are shown in Fig.S2. It is evident from the figures that the intermolecular interaction depicted by d_{norm}, shape index and curvedness indicates similar results as obtained in case of the compound consisting of three monomers. The percentage of each atom-atom interaction obtained from FP plots are almost similar to the results of polymer chain with three molecules. Thus it can be concluded that the number of molecules present in the polymer chain do not alter the results of Hirsfeld surface analysis.

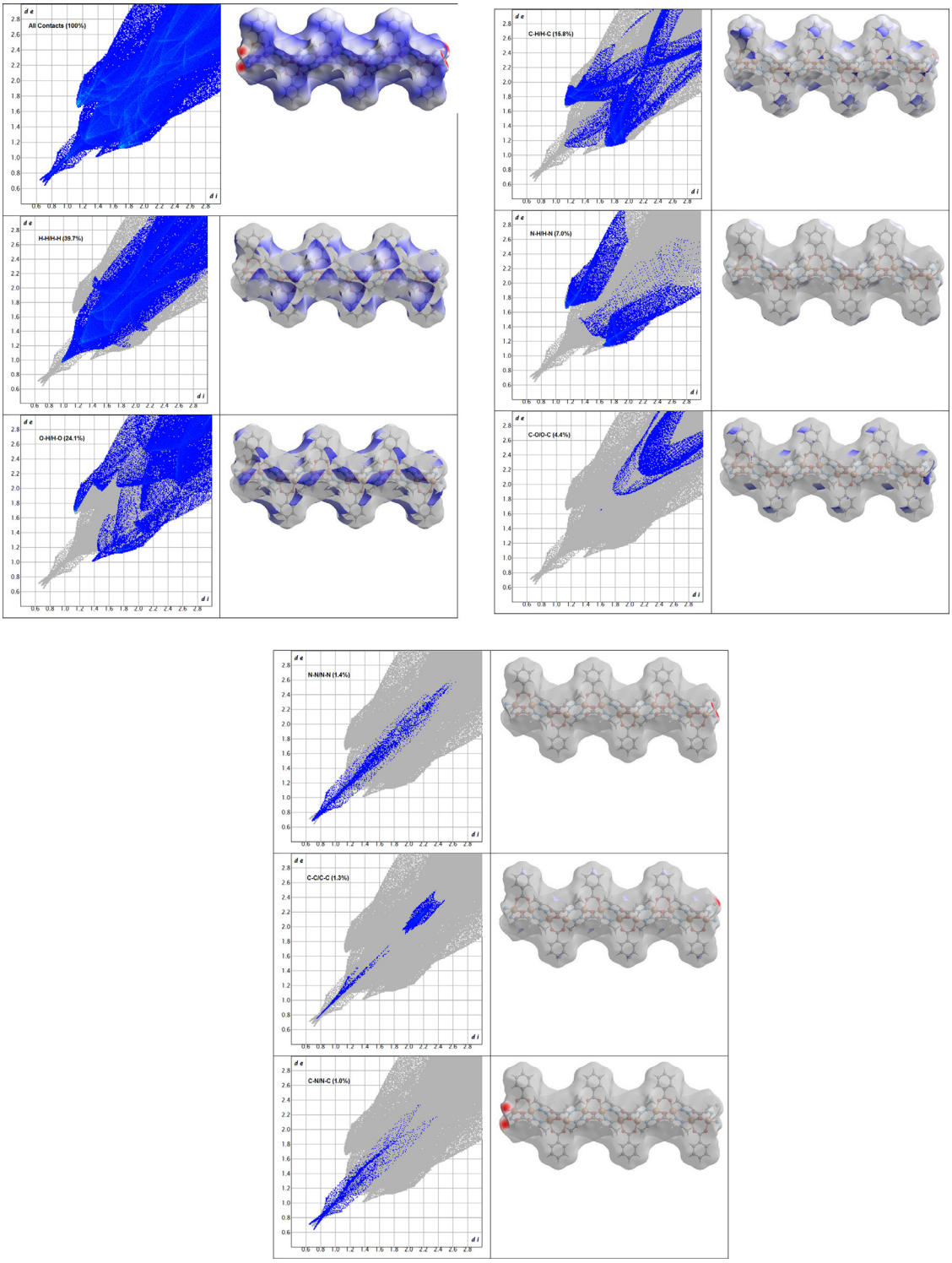

Fig. 6. Two-dimensional fingerprint plot for the compound showing the contributions of individual interactions: Outline of the full fingerprint is shown in grey. Surfaces to the right highlight the relevant surface patches associated with the specific contacts with d_{norm} mapped.

4. Conclusion

We have synthesized a new Cu(II) 1D coordination polymer using a pyrazole based ligand accompanied by auxiliary ligand benzoic acid. In the crystal structure of complex **1**, Cu(II) shows distorted trigonal bipyramidal in geometry. The DFT optimized structure is in accordance with the X-ray crystallography structure. The hardness value of the global reactivity parameter suggests the complex to less reactive chemically. The colour code on the MEP surface also indicates the complex to be not highly reactive; however it will exhibit electrophilic reactvity through the crboxyl group attached with the pyrazole ring. The Hirshfeld surface demonstrates H···H and O···H interaction contributing 39.7% and 24.1% respectively towards crystal packing. The result reported here might be useful in understanding similar kind of polymeric complex.

Declaration of Competing Interest

The authors declare that they have no known competing financial interests or personal relationships that could have appeared to influence the work reported in this paper.

The authors declare the following financial interests/personal relationships which may be considered as potential competing interests:

CRediT authorship contribution statement

Mridula Guin: DFT calculation and written its part. **Shibashis Halder**: Written the structural description of complex. **Sudipta Chatterjee**: Crystal structure determination. **Saugata Konar**: Writing - original draft, Conceptualization, Data curation, Investigation, Methodology.

Data Availability

I have shared the data mentioned in reference list

Acknowledgements

S. K. is thankful to The Bhawanipur Education Society College, Kolkata 700020 for providing research grant (Project No. BESC/RPC/2019–2020/SC1/02). The authors are highly grateful to the Sharda University, Greater Noida, for providing Gaussian 16 for the DFT calculations to accomplish this study.

Supplementary materials

CCDC 1,011,220 contains the supplementary crystallographic data for **1**. These data can be obtained free of charge *via*http://www.ccdc.cam.ac.uk/conts/retrieving.html, or from the Cambridge Crystallographic Data Centre, 12 Union Road, Cambridge CB2 1EZ, UK; fax: (+44) 1223–336–033; or e-mail: deposit@ccdc.cam.ac.uk.

Supplementary material associated with this article can be found, in the online version, at doi:10.1016/j.molstruc.2022.133949.

References

[1] A.G. Wong-Foy, A.J. Matzger, O.M. Yaghi, Exceptional H_2 saturation uptake in microporous metal−organic frameworks, J. Am. Chem. Soc. 128 (2006) 3494–3495.
[2] Y. Zhao, D.-S. Deng, L.-F. Ma, B.-M. Ji, L.-Y. Wang, A new copper-based metal–organic framework as a promising heterogeneous catalyst for chemo- and regio-selective enamination of β-ketoesters, Chem. Commun. 49 (2013) 10299–10301.
[3] M.M. Wanderley, C. Wang, C.-D. Wu, W.-B. Lin, A chiral porous metal–organic framework for highly sensitive and enantioselective fluorescence sensing of amino alcohols, J. Am. Chem. Soc. 134 (2012) 9050–9053.
[4] D.-S. Li, P. Zhang, J. Zhao, Z.-F. Fang, M. Du, K. Zou, Y.-Q. Mu, Two unique Entangling Cd^{II}-Coordination Frameworks Constructed by Square Cd_4-BUILDING Blocks and Auxiliary N,N′-Donor ligands, Cryst. Growth Des. 12 (2012) 1697–1702.
[5] X.-M. Zhang, Z.-M. Hao, W.-X. Zhang, X.-M. Chen, Dehydration-induced conversion from a Single-Chain Magnet into a Metamagnet in a Homometallic nanoporous metal–organic framework, Angew. Chem., Int. Ed. 46 (2007) 3456–3459.
[6] D.-S. Li, J. Zhao, Y.-P. Wu, B. Liu, L. Bai, K. Zou, M. Du, Co_5/Co_8–cluster-based coordination polymers showing high-connected self-penetrating networks: syntheses, crystal structures, and magnetic properties, Inorg. Chem. 52 (2013) 8091–8098.
[7] Y.-L. Wang, J.-H. Fu, J.-J. Wei, X. Xu, X.-F. Li, Q.-Y. Liu, Noncentrosymmetric organic solid and Its Zinc coordination polymer with diamonded network prepared from an lonothermal reaction: syntheses, crystal structures, and second-order nonlinear optics properties, Cryst. Growth Des. 12 (2012) 4663–4668.
[8] J.Y. Seo, S.H. Lee, M. Jazbinsek, H. Yun, J.T. Kim, Y.S. Lee, I.H. Baek, F. Rotermund, O.P. Kwon, New Thiolated Nitrophenylhydrazone crystals for nonlinear optics, Cryst. Growth Des. 12 (2012) 313–319.
[9] L. Du, Z. Lu, K. Zheng, J. Wang, X. Zheng, Y. Pan, X. You, J. Bai, Fine-tuning pore size by shifting coordination sites of ligands and surface polarization of metal–organic frameworks to sharply enhance the selectivity for CO_2, J. Am. Chem. Soc. 135 (2013) 562–565.
[10] L.J. Murray, M. Dinca, J. Yano, S. Chavan, S. Bordiga, C.M. Brown, J.R. Long, Highly-selective and reversible O_2 binding in Cr_3(1,3,5-benzenetricarboxylate)$_2$, J. Am. Chem. Soc. 132 (2010) 7856–7857.
[11] W.-W. Sun, A.-L. Cheng, Q.-X. Jia, E.-Q. Gao, Metal-coordination-directed assembly of binuclear trigonal prisms and three-dimensional hydrogen-bonded networks, Inorg. Chem. 46 (2007) 5471–5473.
[12] A.W. Kleij, J.N.H. Reek, Ligand-template directed assembly: an efficient approach for the supramolecular encapsulation of transition-metal catalysts, Chem. Eur. J. 12 (2006) 4218–4227.
[13] J.-G. Lin, Y.-Y. Xu, L. Qiu, S.-Q. Zang, C.-S. Lu, C.-Y. Duan, Y.-Z. Li, S. Gao, Q.-J. Meng, Ligand-to-metal ratio controlled assembly of nanoporous metal–organic frameworks, Chem. Commun. (2008) 2659–2661.
[14] M. Du, X.-G. Wang, Z.-H. Zhang, L.-F. Tang, X.-J. Zhao, Solvent-directed layered Co(II) coordination polymers with unusual solid-state properties: from a nanoporous framework to the dense polythreading 3-D aggregation, CrystEngComm 8 (2006) 788–793.
[15] C.-M. Liu, S. Gao, D.-Q. Zhang, D.-B. Zhu, Three-dimensional eight- or four–connected metal−organic frameworks tuned by hydrothermal temperatures, Cryst. Growth Des. 7 (2007) 1312–1317.
[16] C. Liu, F. Luo, W. Liao, D. Li, X. Wang, R. Dronskowski, pH-dependent syntheses and structures of two Copper(II)/Phenanthroline/p-Sulfonatocalix[4]arene supramolecular compounds with 1D water-filled channels, Cryst. Growth Des. 7 (2007) 2282–2285.
[17] G. Mahmoudi, A. Morsali, Counter-ion influence on the coordination mode of the 2,5-bis(4-pyridyl)-1,3,4-oxadiazole (bpo) ligand in mercury(II) coordination polymers, $[Hg(bpo)_nX_2]$: x = I^-, Br^-, SCN^-, N_3^- and NO_2^-; spectroscopic, thermal, fluorescence and structural studies, CrystEngComm 9 (2007) 1062–1072.
[18] Y.-P. Wu, D.-S. Li, F. Fu, W.-W. Dong, J. Zhao, K. Zou, Y.-Y. Wang, Stoichiometry of N-donor ligand mediated assembly in the Zn^{II}-Hfipbb system: from a 2-Fold interpenetrating pillared-Network to Unique (3,4)-Connected isomeric nets, Cryst. Growth Des. 11 (2011) 3850–3857.
[19] S. Konar, A. Jana, K. Das, S. Ray, S. Chatterjee, S.K. Kar, Three new 1D Cu(II) coordination polymers and a binuclear Cu(II) complex of two pyrazole derived Schiff base ligands: heterocyclic ring substitution and anion dependent structural variations – Spectral studies, Inorganica Chim. Acta 395 (2013) 1–10.
[20] S. Konar, U. Saha, M. Dolai, S. Chatterjee, Synthesis of 2D polymeric dicyanamide bridged hexa-coordinated Cu(II) complex: structural characterization, spectral studies and TDDFT calculation, J. Mol. Struct. 1075 (2014) 286–291.
[21] M.A. Spackman, &D. Jayatilaka, Hirshfeld surface analysis, CrystEngComm 11 (2009) 19–32.
[22] D.L. Smith, A.A. Forist, W.E. Dulin, 5-Methylpyrazole-3-carboxylic acid. The potent Hypoglycemic metabolite of 3,5-Dimethylpyrazole in the Rat, J. Med. Chem. 8 (1965) 350–353.
[23] APEX-II, SAINT and SADABS, Bruker AXS Inc., Madison, WI, 2008.
[24] G.M. Sheldrick, SHELXT - Integrated space-group and crystal-structure determination, Acta Cryst. A 71 (2015) 3–8.
[25] G.M. Sheldrick, Crystal structure refinement with SHELXL, Acta Crystallogr., Sect. C: Cryst. Struct. Commun. 71 (2015) 3–8.
[26] M.J. Frisch, G.W. Trucks, H.B. Schlegel, G.E. Scuseria, M.A. Robb, J.R. Cheeseman, G. Scalmani, V. Barone, G.A. Petersson, H. Nakatsuji, X. Li, M. Caricato, A.V. Marenich, J. Bloino, B.G. Janesko, R. Gomperts, B. Mennucci, H.P. Hratchian, J.V. Ortiz, A.F. Izmaylov, J.L. Sonnenberg, D. Williams-Young, F. Ding, F. Lipparini, F. Egidi, J. Goings, B. Peng, A. Petrone, T. Henderson, D. Ranasinghe, V.G. Zakrzewski, J. Gao, N. Rega, G. Zheng, W. Liang, M. Hada, M. Ehara, K. Toyota, R. Fukuda, J. Hasegawa, M. Ishida, T. Nakajima, Y. Honda, O. Kitao, H. Nakai, T. Vreven, K. Throssell, J.A. Montgomery Jr., J.E. Peralta, F. Ogliaro, M.J. Bearpark, J.J. Heyd, E.N. Brothers, K.N. Kudin, V.N. Staroverov, T.A. Keith, R. Kobayashi, J. Normand, K. Raghavachari, A.P. Rendell, J.C. Burant, S.S. Iyengar, J. Tomasi, M. Cossi, J.M. Millam, M. Klene, C. Adamo, R. Cammi, J.W. Ochterski, R.L. Martin, K. Morokuma, O. Farkas, J.B. Foresman, D.J. Fox, Gaussian 16, Revision C.01, Gaussian, Inc., Wallingford CT, 2016.
[27] E.D. Glendening, A.E. Reed, J.E. Carpenter, F. Weinhold, NBO Version 3.1, TCI, University of Wisconsin, Madison, 1998.
[28] M.J. Turner, J.J. McKinnon, S.K. Wolff, D.J. Grimwood, P.R. Spackman, D. Jayatilaka, M.A. Spackman, CrystalExplorer17, The University of Western Australia, 2017.
[29] A.W. Addison, T.N. Rao, J. Reedijk, J. Rijn, G.C. van Verschoor, Synthesis, structure, and spectroscopic properties of Copper(II) compounds containing nitrogen-sulphur donor ligands; the crystal and molecular structure of Aqua[*l*,7-*bis*(N-*methylbenzimidazol*-2′-*yl*)- 2,6-*dithiaheptane*]copper(II) perchlorate, J. Chem. Soc., Dalton Trans. (1984) 1349–1356.
[30] R.G. Pearson, Absolute electronegativity and absolute hardness of Lewis acids and bases, J. Am. Chem. Soc. 107 (24) (1985) 6801–6806.
[31] M. Arora, A. Kaur Jassal, S.K. Chawla, R.K. Mudsainiyan, Cu(II) ion based 1D coordination polymer: its thermal, fluorescence properties, Hirshfeld surface analysis and theoretical calculations, Mol. Cryst. Liq. Cryst. 664 (2018) 142–155.
[32] N. Dissem, P. Kaur, L.K. Rana, T. Maris, A. Duong, Synthesis, characterization and Hirshfeld surface analysis of a mixed–ligand copper (II) coordination poly-

mer from 1,4,8,11–tetraazacyclotetradecane and pyromellitic dianhydride, Transit. Met. Chem. 46 (2021) 283–290.
[33] R.K. Tiwari, I. Shruti, J.N. Behera, Synthesis, structure and the Hirshfeld surface analysis of three novel metal-tiron coordination complexes, RSC. Adv. 11 (2021) 10767.
[34] C.B. Pinto, L.H.R. Dos Santos, B.L. Rodrigues, Understanding metal–ligand interactions in coordination polymers using Hirshfeld surface analysis, C75 (2019) 707–716.
[35] D. Wang, T. Wang, P. Zhao, Z. Shi, Q. Zhao, Physical characterizations, Hirshfeld surface analysis and luminescent properties of Cd(II) and Pb(II) coordination polymers based on 3-(1,2,4-triazol-1-yl)-benzoic acid, Inorg. Chim. Acta. 508 (2020) 119657.
[36] S.Khanna M.Guin, S.B. Elavarasi, P. Sarkar, DFT calculation, Hirshfeld surface analysis and docking studies of 3-anisaldehyde thiosemicarbazone, J. Chem. Sci. 132 (81) (2020) 1–11.
[37] S.J. Munshi, M.H. Sadhu, M. Guin, S.B. Kumar, Synthesis, structure and molecular hirshfeld surface analysis of Polymeric Cadmium(II) complex involving tetradentate N3S-donor ligand and dicyanamide as bridging ligand, Indian J. Chem. Sec A: IJC 60A (2021) 663–668.
[38] S.J. Munshi, M. Guin, S. Kundu S. B. Kumar, Synthesis, structures and Hirshfeld surface analysis of Ni(II) and Co(III) complexes with N_2O donor Schiff base ligand, J. Indian Chem. Soc 98 (2021) 100080.